Solvent-Induced Crystallization in Poly(ethylene terephthalate) during Mass Transport: Mechanism and Boundary Condition

ARTICLE *in* MACROMOLECULES · SEPTEMBER 2004

Impact Factor: 5.8 · DOI: 10.1021/ma0400416

5 AUTHORS, INCLUDING:

Handong Ouyang
National Tsing Hua University
75 PUBLICATIONS **674** CITATIONS

SEE PROFILE

Tzong-Ming Wu
National Chung Hsing University
123 PUBLICATIONS **2,509** CITATIONS

SEE PROFILE

Solvent-Induced Crystallization in Poly(ethylene terephthalate) during Mass Transport: Mechanism and Boundary Condition

Hao Ouyang,*,† Wen-Hao Lee,† Wen Ouyang,‡ Sham-Tsong Shiue,† and Tzong-Ming Wu†

Department of Materials Engineering, National Chung Hsing University, 250, Kuo Kuang Rd., Taichung 402, Taiwan, R.O.C., and Department of Computer Science and Information Engineering, Chung-Hua University, 707, Sec. 2, WuFu Rd., Hsinchu, Taiwan 300, R.O.C.

Received February 18, 2004

ABSTRACT: The mechanism of mass transport and the related crystallization in poly(ethylene terephthalate) (PET) were studied. Solvent-induced crystallization can occur during the transport process in PET at low temperature. The important effect of changing the surrounding medium to solvent molecules is to reduce the glass transition temperature. This phenomenon is called "plasticization". The extent of plasticization relies on the amount of solvent around the polymer molecules, i.e., the concentration of solvent which will depend on the mass transport before saturation. Evidences for the transport mechanism in the first stage of crystallization were revealed. The distinct diffusion front was determined from the measurements of optical microscope and microhardness. The differential scanning calorimeter (DSC) curves displayed crystallization exothermic peaks whose areas decreased with the amounts of amorphous regions, representing the solvent-induced crystallization (SINC) process. The observed phenomenon of multiple-stage crystallizations is associated with the variation of boundary conditions during mass transport, which was ignored in most theoretical analyses.

Introduction

Introduction of an interactive organic solvent with low molecular weight can induce crystallization in glassy poly(ethylene terephthalate) (PET) by plasticizing the material. The important effect of changing the surrounding medium to solvent molecules is to lower the relaxation time and therefore to depress the glass transition temperature due to the additional free volume introduced with the diluent molecules.[1] Therefore, the sufficient soluble acetone in amorphous PET adopted in this work will help the chains inside the polymer surmount the activation barrier to attain the more stable state: the crystalline state. The degree of plasticization depends on the amount of solvent inside, and the behavior of crystallization is closely related to the mechanism of mass transport. Therefore, it is important to understand the transport behavior in detail for the study of solvent-induced crystallization. The early work on solvent-induced crystallization concentrated on the crystallization in interactive liquids of PET films of moderate thickness and observed that penetrant transport controls the crystallization process.[2−4] Recently, it was found that the crystallization processes can be divided into three stages, and the crystallization can proceed without considering the influence of mass transport only in the last stage.[5] The first two stages can be assorted as the "primary crystallization", and the last process is related to the "secondary crystallization". The discussion of details of multiple-stage processes relating to the mechanism of solvent transport was presented in this work. The transport of organic solvents in the glassy polymer has been sorted by Alfrey et al. to include the case I (Fickian) and case II (swelling mechanisms).[6] Anomalous diffusion is a combination of case I and case II. When the kinetics is dominated by case I, the penetration distance is proportional to the square root of time, $t^{1/2}$, and the diffusion distance is proportional to t for the prevalence of case II.[7] Kwei et al.[8−11] proposed a mathematical model to explain case I and case II transport phenomena in finite and semi-infinite media.

Harmon et al.[12,13] explored the transport behavior of methanol in a deformed, cross-linked poly(methyl methacrylate) (PMMA) using a modified Kwei's equation. About the same period Perterlin presented a transport model under the assumption of discontinuous swelling.[14] Durning et al.[15−18] included the effect of crystallization in the behavior of mass transport with the assumption of constant surface concentration during the sorption. Zachmann and Konrad applied a modified Avrami-type analysis in the study of solvent-induced crystallization (SINC).[19] The correct descriptions of transport phenomena for all kinds of models rely on accurate and correct assumptions. This work will provide more detail about the boundary conditions and transport behavior based on experimental observations.

Experimental Section

This study involves experimental observations of acetone absorption, differential scanning calorimetry (DSC), optical microscopy (OM), microscopic Fourier transform infrared (FTIR) spectroscopy, and microhardness measurements. The amorphous PET (ES301465) sheet was ordered from the Goodfellow Co., Cambridge, England. All specimens were prepared as follows. Samples with the size of 10 × 3 × 0.25 mm were cut from the sheet and polished using 800, 1200, 1500, and 4000-grid carbimet papers, then were annealed in a vacuum of 10^{-3} Torr for 4 h at 70 °C, and immediately furnace-cooled to the ambient temperature, around 23 °C. Final polishing with 1, 0.5, and 0.05 μm alumina slurries was followed. The thickness of the sample for further experimental work is about 0.23 mm, which is less than one-tenth of the other dimensions. Then they were annealed again in a vacuum of 10^{-3} Torr for 4 h at 70 °C and furnace-cooled to the ambient

† National Chung Hsing University.
‡ Chung-Hua University.
* To whom correspondence should be addressed: Tel (04)-2285-2801; FAX (04)-2285-7017.

10.1021/ma0400416 CCC: $27.50
Published on Web 09/03/2004

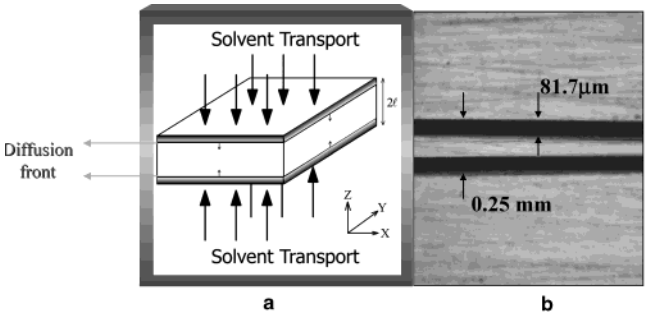

Figure 1. (a) Schematic plot of solvent transport. (b) Example of OM showing the view of cross section.

temperature. This thermal treatment was performed in an EYELA VOS-200SD vacuum oven to reduce the degree of subsequent shape deformation without causing degradation of the polymer. All the treated samples were dried in a vacuum desiccator for 3 days at room temperature to remove the remaining solvent.

Absorption Measurement. Each absorption sample was preheated at the same sorption temperature in a vacuum for 15 min and then put in a glass test tube filled with acetone at 50 °C. The detailed procedures were described in ref 20. To understand the evolution process of crystallization and mass transport, many specimens with almost the same dimension were prepared in identical procedures and removed at different treated times during the absorption experiment and then kept in a vacuum furnace of 10^{-3} Torr at room temperature for 3 days. Basically each data point represents a fresh specimen. Once a sample had been measured, it was not reimmersed and reused.

DSC Measurement. Thermal analysis of the samples was performed using a Perkin-Elmer PYRIS Diamond differential scanning calorimeter (DSC) calibrated using indium, and all experiments were carried out under a nitrogen atmosphere. The specimens were obtained by cutting a rectangular parallelepiped of 3.5 × 2 × 0.3 mm from a solvent-saturated sample after staying in a vacuum desiccator for 3 days. The purpose for using a relatively small sample thickness was to reduce the effect of low thermal conductivity of the polymers. All specimens had weights in the range of 2−3 mg and were heated from 25 to 350 °C at a rate of 10 °C/min. The initial development of solvent-induced crystallization was observed as the area under the crystallization peak became smaller and smaller with increasing solvent-treated time.

Optical Microscopy Measurement. The transport fronts and traveling distances can be examined in an Olympus BX60 optical microscopy since the material becomes opaque as the solvent immigrates into PET and causes crystallization. The solvent-treated sample was cold-mounted employing the Struers Speci Fix-20 and left at room temperature for 8 h. Afterward, the sample was sectioned by a Struers Minitom and then polished to reveal its cross section as shown in Figure 1a observed along the *x*-direction.

Microhardness Measurement. Microhardness was measured at room temperature using a Future-Tech FM-7 digital tester with a Vickers square pyramidal diamond indenter. The HV value can be obtained from the residual projected impression using the equation

$$\mathrm{HV} = Kp/d^2 \qquad (1)$$

where d is the mean diagonal length of the indentation, p is the applied force, and K is a geometrical factor.[21] A load cycle of 35 s was adopted to minimize the influence of creep of the material under the indenter. The length of the impression was measured with a microscope equipped with a filar eyepiece.

Microscopic FTIR Spectroscopic Measurement. The microscopic FTIR spectroscopic measurement was performed in a Bruker IFS48 microscope with a 0.04 mm aperture. The spectrum of the empty cell was collected first as for the background correction. The scanning range was from 4000 to 600 cm^{-1}, and the resolution is 4 cm^{-1} after computer-averaging a total of 100 scans. In PET, the band at 973 cm^{-1} was explained as the asymmetric C−O stretching mode and can be related to the trans conformation of the −O−C−C−)− group.[22−24] The intensity of this band is very sensitive to the crystallinity of the polymer.[22,23,25] One of reasons for adopting this band for later analysis is that the peak at 973 cm^{-1} can be clearly identified through the transmission mode even when the sample is pretty thick (around 0.3 mm). The conformationally insensitive band at 795 cm^{-1} was used as an internal thickness standard.[22,26] Therefore, the variation of the relative intensity of the absorption band at 973 cm^{-1} can be quantified to monitor the change of crystallinity in terms of the reduced factor which was obtained from the peak area associated with the 973 cm^{-1} band normalized by that of the 795 cm^{-1} band.[22] The detailed procedures can be referred to our previous work.[20]

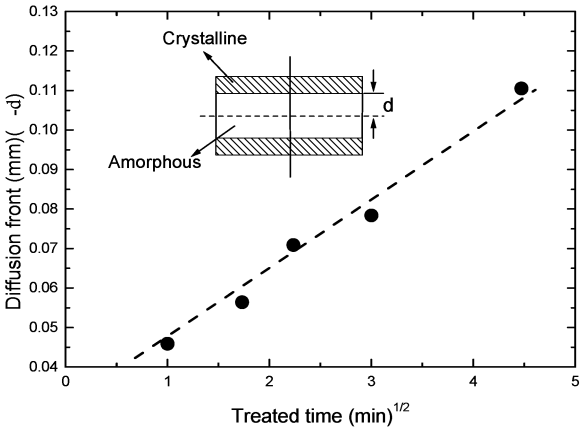

Figure 2. Solvent traveling distance, $l_0 - d$, vs square root of time, the inset representing how to obtain d; the dotted line is drawn to show a linear relationship.

Results and Discussion

When the transport mechanism is dominated by case I, the diffusion front is proportional to the square root of time, $t^{1/2}$, whereas the traveling distance of front is proportional to t for the prevalence of case II.[7] The OM can reveal the transport front vs time as the example presented in Figure 1b since the transparent amorphous region became opaque after crystallization. The traveling distance, $l_0 - d$, is proportional to $t^{1/2}$ before the merge of fronts as presented in Figure 2. Here l_0 is the original half-thickness and d is the half-width of glassy core. DSC exploring the amount of residual amorphous phase was performed as represented in Figure 3. The degree of solvent-induced crystallization could be estimated from the smaller area of the crystallization peak (peak 2 in the figure) with increasing solvent-treated time.[7] Peak 2 basically represents the amount of glassy core, and the transition of this area or specific enthalpy also obeys the law of $t^{1/2}$ as shown in Figure 4. We used two methods to calculate the peak areas. After the subtraction of background, the peak areas can be obtained either by assuming the shape of peak 1 as we computed the peaks of infrared spectra before,[20] then integrated the whole area above the background as presented in the plot, or by fitting the curve with two Lorentzians. The results from both peak-calculating methods all follow the relationship of square root of time. It has been shown that the penetrant transport controlled the extent of induced crystallization in this system.[2−5] Therefore, case I dominated during the transport process in this stage until the diffusional tails from opposite sides start overlapping considerably. The gradual transition to lower temperature for peak 2 can

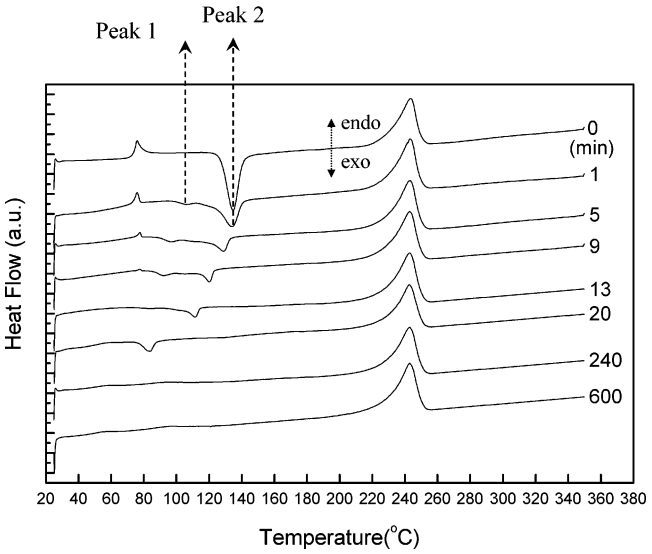

Figure 3. DSC curves of PET solvent-treated at different periods.

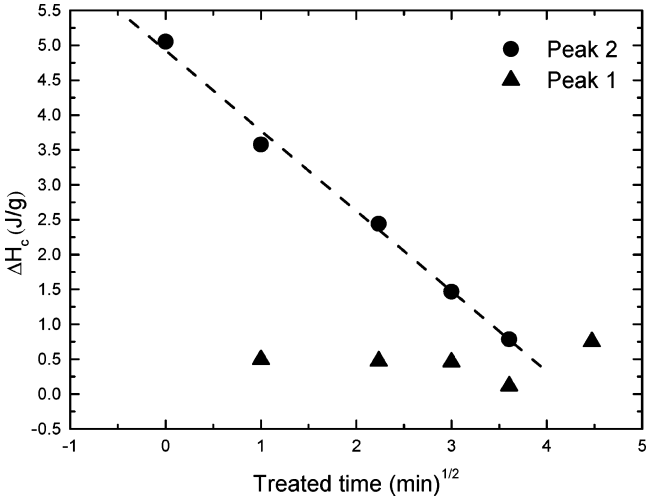

Figure 4. Specific enthalpies from the area of peak 1 and 2 vs square root of time; the dotted line is drawn to show a linear relationship.

be interpreted as the result of the characteristic Fickian diffusional tail of acetone concentration, and the occurrence of crystallization is getting easier with the existence of some solvent. The time for the acetone diffusion fronts to reach the middle of the sample as observed by OM also corresponds to that of the SINC observed from peak 2 by DSC. However, peak 1 observed from DSC increased dramatically after the merge of diffusion fronts, which reflects the ability of further crystallization from the region of solvent-induced transformation since it appears after the merge of transport front. This increase is consistent with our previous result that the swelling activated afterward, and most of the crystallization occurs in this stage.[5] Therefore, the behavior of peak 1 also implies that the ability of crystallization is different after the diffusion fronts impinge upon each other considerably, and more details will be discussed later.

As mentioned above, the transport mechanism controlled the process of solvent-induced crystallization, and the amount of solvent residing in PET will affect the degree of crystallization. Therefore, it is possible to obtain information about the solvent-concentration

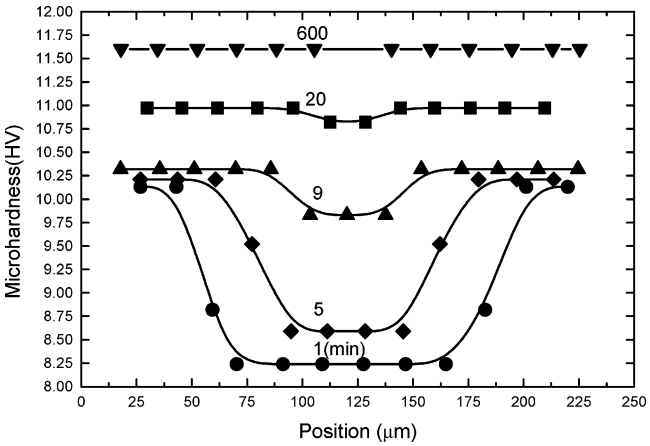

Figure 5. HV values at different solvent-treated periods vs positions on the cross section; the solid lines are drawn to show the distribution of microhardness.

distribution from the measurement of crystallization at different positions on the cross section of the samples.

The microhardness observation has become a physical method that provides quantitative information on changes in the morphology of polymers in recent years.[27−29] It has been shown that the value of HV increases during the evolution of the primary crystallization.[29] This result was discussed in terms of three important morphological elements: the crystalline lamellae, the intercrystalline disordered layers, and the interspherulitic amorphous regions. The expression which offers a useful description of the microhardness of PET in relation to these three morphological features can be written as[29]

$$HV = [HV_c\phi_c^{lin} + HV_a(1 - \phi_c^{lin})]\phi + HV_a(1 - \phi) \quad (2)$$

$$= HV_{sph}\phi + HV_a(1 - \phi) \quad (3)$$

$$= (HV_{sph} - HV_a)\phi + HV_a \quad (4)$$

where HV_c is the crystal hardness, ϕ_c^{lin} the linear crystallinity, HV_a the microhardness of the amorphous glassy material, and ϕ the volume fraction of lamellae; HV_{sph} is equal to $[HV_c\phi_c^{lin} + HV_a(1 - \phi_c^{lin})]$. The linear relationship between HV and ϕ can be found from eq 4 if HV_c, ϕ_c^{lin}, and HV_a remain constants. In fact, it has been shown that the value of HV increases linearly with the macroscopic density or crystallinity for the semicrystalline PET during the primary crystallization.[29,30] Therefore, microhardness measurements could accurately detect the gradual transformation in the region of interest, and this method can be employed to observe the crystallization distribution by measuring the HV values at different positions of cross section mentioned above, as shown in Figure 5. To confirm the above argument, that the degree of crystallization is proportional to the HV value, applicable in this study, microscopic FTIR spectroscopic analysis was utilized to reexamine the local crystallinity of some data by measuring the trans intensity, and the profile is presented in Figure 6. Both results from microhardness and trans measurements are consistent qualitatively. Quantitative differences can be due to different reposnses of optics and mechanics for the residual solvent.[20] Before the merge of diffusion fronts, the profiles of HV value vs sample position can be explained in terms of the standard distribution of Fickian diffusion, and the value

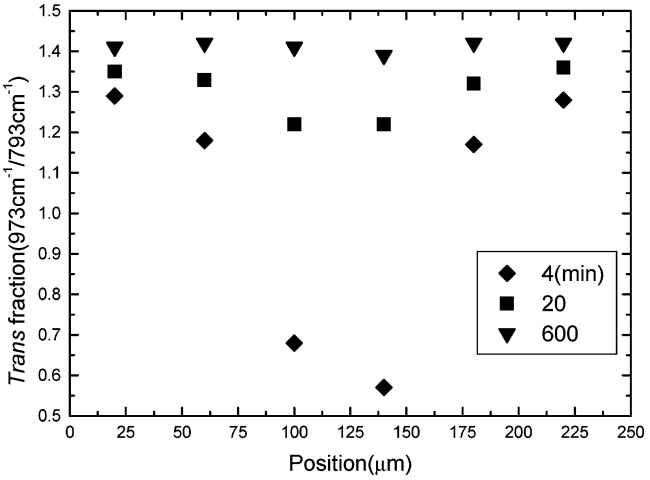

Figure 6. Normalized trans values at different solvent-treated periods vs positions on the cross section.

of HV close to the surface is about the same in this period. After obvious overlap of difusion tails, the value around the surface starts increasing dramatically as shown in the plot. Since the solvent transport controlled the crystallization process in this study, this implies that the boundary condition of constant surface concentration adopted for almost all the theoretical works needs to be modified after the first stage of crystallization. This phenomenon can be explained in terms of the relaxation of hydrostatic stress component on the swollen layer as the diffusion tails starts covering each other sufficiently to remove the constraint from the glassy core. This will cause an increase of "equilibrium" solvent uptake and therefore an increase of crystallinity around the surface. This increase has been explained in terms of thermodynamic equations incorporating the influence of deformation in the rubbery system.[31,32] In fact, during the absorption experiment, it was found that the sample was pretty soft, and the thickness varied dramatically after the end of first stage in our previous invetigation.[5] Litttle influence of solvent-induced crystallization on the "equilibrium" solvent concentration was found at least in the first stage for this study. This can be told from the observation that the HV value around the surface remains almost constant during the first period. The chemical potential per mole of diluent sorbed into a swollen polymer with reference to a standard state is[33,34]

$$\mu_1 - \mu_1^0 = RT\left\{\frac{G\bar{V}_1}{V_i}[(1-\nu_1)^{1/3} - (1-\nu_1)] + \ln \nu_1 + (1-\nu_1) + \chi(1-\nu_1)^2\right\} \quad (5)$$

where G is the number of network segments in the polymer, $\bar{V}_1$ is the molecular volume of diluent, V_i is the volume of unswollen polymer, ν_1 is the volume fraction of diluent in the swollen polymer, and χ is the polymer−solvent interaction parameter. The first term on the right-hand side represents the entropic constraint of the molecular network, and the final three terms are due to the solutions as one component is macromolecular. The microstructure of solvent-induced crystallization is different from that of thermal crystallites and is similar to the amorphous state in the beginning as we discovered from the results of transmission electron microscopy. This is also consistent with former study of X-ray scattering.[20] Therefore, G and χ are expected to be constants, and the concentration of diluent around the surface remains the same at this stage. After this stage, the relaxation of hydrostatic stress component on the swollen layer dominates as the sample thickness was observed to increase dramatically in the second stage,[5] and this causes the raise of "equilibrium" solvent uptake. As the swelling enlarges and solvent concentration is getting higher, the crystallinity increases as shown in Figure 5 due to lower glass transition temperature and compressive strain.[20,35] An increase in crystallinity usually decreases the solubility,[36] which is not observed during the transport process. Therefore, it is the stress relaxation responsible for the increase of "equilibrium" solvent concentration. One feasible model can be proposed by applying a time-dependent boundary condition in the existing model.[15] Consider a PET film of thickness $2l$ and the film area much larger than the lateral area so that a one-dimensional transport model was treated.

The mass conservation obeys the following equation:[15]

$$\frac{\partial(1-\alpha)C}{\partial t} = \frac{\partial}{\partial x} D \frac{\partial C}{\partial x} + \frac{\partial}{\partial x}(1-\alpha)vC \qquad \text{for } 0 < x < l \quad (6)$$

where α is the volume fraction crystallized and C the solvent concentration.

In original work, people assume that the concentration of solvent at boundary surfaces $x = \pm l$ is kept constant at all times, and initially the film is free of solvent. The diffusion coefficient D and velocity v represent the parameters of case I and case II, respectively. By solving eq 6, Harmon et al. obtained an analytical solution of weight gain at time t for α being zero.[12] When the kinetics is dominated by case I, the sorption is proportional to the square root of time, $t^{1/2}$, whereas the mass uptake is proportional to t for the prevalence of case II. The exponent will be between 0.5 and 1 for the anomalous diffusion. However, if the solvent-induced crystallization is considered (α not zero), the introduction of α will block the transport. The transport parameters like diffusion coefficient D and mass average velocity v are expected to change dramatically after the overlap of diffusion fronts. This is due to the fact that the boundary conditions of surface concentration and sample thickness vary with time after the first stage.

Summary

Acetone transport in poly(ethylene terephthalate) and related crystallization process have been investigated. Some important phenomena are summarized as follows:

1. The first stage of crystallization was found to be controlled by the Fickian transport according to the measurements of OM and DSC. This further confirms that crystallization rate in this period is not due to the effect of surface cavitation mentioned in other work.[16] The influence of such effect can be ignored in this study.[37]

2. The results of microhardness and microscopic IR measurements can be used to explore the distribution of solvent concentration since the crystallization behavior is strongly affected by the mass transport in this study.

3. The increase of "equilibrium" solvent uptake after the first stage was caused by the relaxation of con-

straint. This phenomenon has usually being neglected in most theoretical work and causes deviation as compared to experimental results.[7]

The principal result discovered in this work is that crystallinity behind the diffusion front increases suddenly and markedly as the concentration fields of fronts moving from opposite surfaces begin to overlap. This increase in crystallization rate can be understood in terms of swelling effect since the sample dimension increased quite dramatically after the overlap.[5] This shape variation corresponds to the release of internal stress as a result of the relaxation of constraint and in general is thought to be the cause of case II.[20] Such stress relaxation causes greater surface solvent concentration, subsequently enhances the mobility of polymer chain,[1] and promotes a faster rate of crystallization. The above argument is also consistent with the fact that case II was found to prevail at higher solvent concentration.[6]

Acknowledgment. This work was supported by the National Science Council, Taiwan, Republic of China. The authors thank Chung-Hua Telecommunication Laboratories for lending the FTIR microscope.

References and Notes

(1) Ferry, J. D. *Viscoelastic Properties of Polymers*, 3rd ed.; Wiley: New York, 1980; Chapter 17.
(2) Moore, W. R.; Sheldon, R. P. *Polymer* **1961**, *2*, 315.
(3) Cottam, L.; Sheldon, R. P. *Adv. Polym. Sci. Technol.* **1966**, *26*, 65.
(4) Desai, A. B.; Wilkes, G. L. *J. Polym. Sci., Polym. Symp.* **1974**, *46*, 291.
(5) Ouyang, H.; Lee, W.-H.; Shih, M.-C. *Macromolecules* **2002**, *35*, 8428.
(6) Alfrey, T.; Gurnee, E. F.; Lloyd, W. G. *J. Polym. Sci., Part C* **1966**, *12*, 249.
(7) Cornélis, H.; Kander, R. G. *Polymer* **1996**, *37*, 5627.
(8) Wang, T. T.; Kwei, T. K.; Frish, H. L. *J. Polym. Sci., Part A-2* **1969**, *7*, 2019.
(9) Kwei, T. K.; Wang, T. T.; Zupko, H. M. *Macromolecules* **1972**, *5*, 645.
(10) Kwei, T. K.; Zupko, H. M. *J. Polym. Sci., Part A-2* **1969**, *7*, 867.
(11) Wang, T. T.; Kwei, T. K. *Macromolecules* **1973**, *6*, 919.
(12) Harmon, J. P.; Lee, S.; Li, J. C. M. *J. Polym. Sci., Part A: Polym. Chem.* **1987**, *25*, 3215.
(13) Harmon, J. P.; Lee, S.; Li, J. C. M. *Polymer* **1988**, *29*, 1221.
(14) Perterlin, A. *Makromol. Chem.* **1969**, *124*, 136.
(15) Durning, C. J.; Russel, W. B. *Polymer* **1985**, *26*, 119.
(16) Durning, C. J.; Russel, W. B. *Polymer* **1985**, *26*, 131.
(17) Durning, C. J.; Rebenfeld, L.; Russel, W. B.; Weigmann, H. D. *J. Polym. Sci., Part B: Polym. Phys.* **1986**, *24*, 1321.
(18) Durning, C. J.; Rebenfeld, L.; Russel, W. B.; Weigmann, H. D. *J. Polym. Sci., Part B: Polym. Phys.* **1986**, *24*, 1341.
(19) Zachmann, H. G.; Konrad, G. *Makromol. Chem.* **1968**, *118*, 189.
(20) Ouyang, H.; Lee, W.-H.; Shiue, S.-T.; Lin, T.-L. *J. Polym. Sci., Part B: Polym. Phys.* **2002**, *40*, 1444.
(21) Baltá Calleja, F. J.; Martínez, S. J.; Rueda, D. R. *Encyclopedia of Polymer Science engineering*; Wiley-Interscience: New York, 1986: Vol. 6, p 614.
(22) Ito, M.; Pereira, J. R. C.; Hsu, S. L.; Porter, R. S. *J. Polym. Sci., Polym. Phys. Ed.* **1983**, *21*, 389.
(23) Miyake, A. J. *Polym. Sci.* **1959**, *38*, 479.
(24) Hannon, M. J.; Koenig, J. L. *J. Polym. Sci., Part A-2* **1969**, *7*, 1085.
(25) Aharoni, S. M.; Sharma, R. K.; Szobota, J. S.; Vernick, D. A. *J. Appl. Polym. Sci.* **1983**, *28*, 2177.
(26) Cunningham, A.; Ward, I. M.; Willis, H. A.; Zichy, V. *Polymer* **1974**, *15*, 749.
(27) Baltá Calleja, F. J.; García Gutirrez, M. C.; Rueda, D. R.; Piccarolo, S. *Polymer* **2000**, *41*, 4143.
(28) Vanderdonckt, C.; Krumova, M.; Baltá Calleja, F. J.; Zachmann, H. G.; Fakirov, S. *Colloid Polym. Sci.* **1998**, *276*, 138.
(29) Santa Cruz, C.; Baltá Calleja, F. J.; Zachmann, H. G.; Stribeck, N.; Asano, T. *J. Polym. Sci., Part B: Polym. Phys.* **1991**, *29*, 819.
(30) Baltá Calleja, F. J.; García Gutirrez, M. C.; Rueda, D. R.; Piccarolo, S. *Polymer* **2000**, *41*, 4143.
(31) Thomas, N. L.; Windle, A. H. *Polymer* **1981**, *627*, 22.
(32) Flory, P. J. *Proc. R. Soc. London* **1976**, *351*, 351.
(33) Smith, K. J. Theories of Chain Coiling, Elasticity and Viscoelasticity. In *Polymer Science;* Jenkins, A. D., Ed.; North-Holland: Amsterdam, 1973; Vol. 1.
(34) Thomas, N. L.; Windle, A. H. *Polymer* **1982**, *23*, 529.
(35) Tashiro, K.; Yoshioka, A. *Macromolecules* **2002**, *35*, 410.
(36) Billmeyer, F. W., Jr. *Textbook of Polymer Science*; Wiley-Interscience: New York, 1984; p 152.
(37) Lee, W.-H.; Ouyang, H.; Shih, M.-C.; Wu, M.-H. *J. Polym. Res.* **2003**, *10*, 133.

MA0400416